Process Safety and Environmental Protection 187 (2024) 962–973

Contents lists available at ScienceDirect

Process Safety and Environmental Protection

journal homepage: www.journals.elsevier.com/process-safety-and-environmental-protection

Surface engineered sustainable nanocatalyst with improved coke resistance for dry methane reforming to produce hydrogen

Subhan Azeem [a], Muddasar Safdar [b,c], Rabya Aslam [d], Bohong Wang [e], Imane Ziani [f,g], Sabah Ansar [h], Farooq Sher [i,*]

[a] Department of Chemical Engineering NFC Institute of Engineering and Technology, Multan, Pakistan
[b] Department of Process and Plant Technology, Brandenburg University of Technology (BTU) Cottbus-Senftenberg, Platz der Deutschen 1, Cottbus 03046, Germany
[c] Department of Chemical Engineering Technology, Government College University Faisalabad (GCUF), Faisalabad 38000, Pakistan
[d] Institute of Chemical Engineering and Technology, University of the Punjab, Lahore 54590, Pakistan
[e] National and Local Joint Engineering Research Center of Harbor Oil and Gas Storage and Transportation Technology, Zhejiang Key Laboratory of Petrochemical Environmental Pollution Control, Zhejiang Ocean University, No. 1 Haida South Road, 316022, Zhoushan, P.R. China
[f] Laboratory of Applied Chemistry and Environment, Department of Chemistry, Faculty of Sciences, Mohammed First University, Oujda 60000, Morocco
[g] International Society of Engineering Science and Technology, Nottingham, United Kingdom
[h] Department of Clinical Laboratory Sciences, College of Applied Medical Sciences, King Saud University, P.O. Box 10219, Riyadh 11433, Saudi Arabia
[i] Department of Engineering, School of Science and Technology, Nottingham Trent University, Nottingham NG11 8NS, United Kingdom

ARTICLE INFO

Keywords:
Methane dry reforming (DRM)
Wet Impregnation
Nickel-Zirconia catalyst
Renewable energy
Sustainable
Green hydrogen
Net Zero

ABSTRACT

The ever-growing carbon-based economy has led to alarming increases in greenhouse gas (GHG) emissions, particularly methane (CH_4) and carbon dioxide (CO_2). These emissions accelerate global warming, pollution and environmental challenges. Methane Dry Reforming (DRM) offers a promising technology to address this issue by converting CH_4 and CO_2 into a valuable syngas ($CO + H_2$) mixture, which is a valuable fuel and a building block for many important chemical reactions (Fischer-Tropsch process). However, finding affordable and environmentally friendly catalysts for large-scale applications remains a critical hurdle. This study delves into the development of stable nickel-zirconia catalysts prepared via impregnation method. The weight percentage of nickel and zirconia was varied to optimize the catalyst's activity by controlling deactivation phenomenon that is a major challenge at higher temperatures during DRM. Various characterization techniques (XRD, FT-IR, SEM-EDX, TGA, TEM and BET) were employed to evaluate synthesized catalysts physio-chemical properties. Additionally, catalytic performance was assessed at temperatures ranging from 550 to 750 °C and a gas hourly space velocity (GHSV) of 72,000 mL/h.g_{cat}. Among tested catalysts, 15% Ni/ZrO_2 displayed remarkable conversion values for both CH_4 (62.9%) and CO_2 (64.9%). Importantly, it exhibited significantly lower weight loss (ca. 15.42%) compared to other variants, indicating better resilience against coke deposition. This enhanced stability can be attributed to synergistic interplay between nickel and zirconia support, effectively suppressing carbon formation. These findings demonstrate potential of 15% Ni/ZrO_2 as a promising catalyst for experimental DRM application. With the obvious high activity and stability, 15% Ni/ZrO_2 candidate serves as an eco-friendly candidate for greenhouse gas conversion into green fuel energy, contributing to a sustainable economy and clean environment.

1. Introduction

The reliance on fossil fuels casts a long shadow over our planet. The continual use of these fuels exacerbates climate change, leading to rising temperatures and causing severe environmental consequences (Oni et al., 2023). The need for clean energy solutions has never been more pressing (Velisoju et al., 2023). Thankfully, researchers are developing viable solutions that leverage modern technologies to mitigate these challenges. While the current pace of development may seem insufficient, especially given increasing frequency of climate disasters, it is crucial to combine and integrate promising, technologically validated projects (Mabaleha et al., 2023). In this pursuit, hydrogen emerges as a

* Corresponding author.
E-mail address: Farooq.Sher@ntu.ac.uk (F. Sher).

https://doi.org/10.1016/j.psep.2024.05.033
Received 19 December 2023; Received in revised form 27 April 2024; Accepted 8 May 2024
Available online 12 May 2024

promising contender due to its renewability, clean combustion, and diverse applications in fuel cells. Its versatility extends beyond biomass and natural gas, as it can even be generated from water and hydrocarbons (Mokheimer et al., 2024). This potential to be a truly beneficial fuel with immense potential as a clean energy source makes hydrogen particularly attractive (Zolghadri et al., 2024).

Unlike traditional combustion engines, where interaction of oxygen and hydrogen releases pollutants, fuel cells offer a cleaner approach (Anzures et al., 2021). In fuel cells, energy release occurs more discretely, resulting in water and heat as harmless by-products. Furthermore, hydrogen-driven societies, with their ever-increasing number of vehicles, demonstrate feasibility of using hydrogen without producing harmful emissions like O_3, CO_2, SO_x, CO, or NO_x. This bodes well for human health and the well-being of society as a whole (Kumar et al., 2024). With its minimal emissions and renewable nature, hydrogen has garnered significant interest as a potentially viable energy vector. Technological advancements in fuel cells have further bolstered its position as a leading contender in the race for clean energy sources (Davies et al., 2024). Dry Reforming of Methane (DRM) presents an exciting avenue for unlocking hydrogen's potential (Mokheimer et al., 2024). This technology converts natural gas, a readily available resource, into a valuable mixture of hydrogen and carbon monoxide (syngas). While managing natural gas carries inherent challenges, significant reduction in greenhouse gas emissions compared to traditional processes makes it a worthwhile pursuit (Zhang et al., 2024).

Synthetic gas comprises H_2 and CO that is an excellent intermediate building block that consumes GHGs and produces valuable products via Fischer-Tropsch reaction (Poursadegh, 2023). Furthermore, technologies like Fischer-Tropsch catalysis utilized the downstream processing of synthetic gas to produce significant value-added synthetic compounds comprising olefins, dimethyl ether and other valuable chemicals (Jahangiri et al., 2023). Here, Eq. (1) represented the main governing reaction for DRM process, whilst Eqs. (2) to (4) are competitive side reactions. The two major reactions i.e. CO disproportionation and decomposition of methane depicted by Eqs. (2) and (3) are prime undesirable contributors for coke formation, together with water gas shift reaction represented via Eq. (4). Endothermic in nature, the methane breakdown process necessitates a higher temperature, but CO disproportionation reaction is exothermic and needs a lower temperature and higher pressure. Due to higher temperature requirement of DRM process causes significant deposition of carbon and sintering of metallically active particles (Taherian et al., 2022; Zhou and Mahinpey, 2023) that subsequently reduces desirable conversion targets.

$$CO_2 + CH_4 \rightarrow 2H_2 + 2CO \ \Delta H^\circ = 248 \text{ kJ/mol} \quad (1)$$

$$2CO \rightarrow CO_2 + C \ \Delta H^\circ = -172 \text{ kJ/ mol} \quad (2)$$

$$CH_4 \rightarrow 2H_2 + C \ \Delta H^\circ = 75 \text{ kJ/ mol} \quad (3)$$

$$CO_2 + H_2 \rightarrow H_2O + CO \ \Delta H^\circ = 41/ \text{ kJ mol} \quad (4)$$

In recent past, suitable supported metallic catalysts have been synthesized and tested for DRM process (Zhang et al., 2022). Precious metals like Rh, Pt and Ru-based catalysts have been examined and have demonstrated outstanding stability and activity at higher temperatures coupled with greater coke resistance (Manan et al., 2022). These catalysts have also shown superior resistance against metal sintering at higher temperatures. Although, with higher activity and high stability, noble metal-based catalysts are not a viable option because of their inadequate availability and higher cost (Wang and Wang, 2022; Kiani et al., 2023). Cheaper metals-based catalysts have shown promise as dry reforming of methane catalysts owing to their widespread availability and lower cost (Guharoy et al., 2021; Ranjekar and Yadav, 2021). However, metal sintering and coke deposition caused non-noble metal-based catalysts to rapidly deactivate at higher temperatures (Gao et al., 2020; Torrez-Herrera et al., 2021). Greater temperatures are required to boost conversion rates since DRM process is endothermic (Bian and Kawi, 2018). The possible reactions during DRM process are listed below (Ibrahim et al., 2021).

Ni-based catalysts hold immense promise for DRM due to their affordability and inherent activity (ul Hasnain et al., 2024). However, their Achilles' heel lies in carbon deposition, which clogs reactors and rapidly deactivates them. Finding the right balance between activity and stability is crucial to unlock their true potential in DRM. Both active Ni phase and support material are critical for maintaining stability and catalytic activity against carbon deposition (Guo et al., 2024). Several key factors influence the performance and activity of DRM catalysts, including particle size, metal-support interaction and support composition (Chen et al., 2020). Ni particle size plays a crucial role. Studies suggest that a diameter of around 2–3 nm is optimal for Ni catalysts used in DRM at temperatures between 500–600 °C and a pressure of 5.0 bar (Vogt et al., 2019). Computational studies have shown that binding between Ni and MgO catalysts can be limited, leading to a lack of synergy and limited active sites (Zuo et al., 2018). However, increasing Ni content on the MgO surface enhances the binding and promotes carbon removal. (Al-Fatesh et al., 2021) investigated the use of a combined La_2O_3-ZrO_2 support for Ni catalysts in DRM. Their findings suggest that this support stabilizes tetragonal ZrO_2 phase and promotes CO_2 interaction with catalyst surface through the presence of amorphous $La_2O_2CO_3$ species. (Mourhly et al., 2020) demonstrated long-term stability and reduced coke formation using mesoporous silica as a support for Ni-based catalysts in DRM. Their results revealed coke formation primarily in the form of carbon nanotubes. (Salehi et al., 2024) investigated Ni/ZrO_2 and Ni/M-Al_2O_3 catalysts for hydrogen generation through CO_2 reforming of glycerol. This research highlights the influence of support materials on catalyst performance.

Nickel has been alloyed with various metals and placed on diverse supports like hydrotalcite, cobalt, silica, potassium, manganese and calcium to address this challenge (Yentekakis et al., 2021; Kwon et al., 2022).

This has led to interest in creating a metal oxide by impregnation method, ultimately assisting a nickel catalyst in DRM process for hydrogen production (Sun et al., 2020). Suitable supports (ZrO_2, SiO_2 and Al_2O_3) were utilized by researchers to synthesize appropriate catalysts for DRM (Usman et al., 2015; Al-Fatesh et al., 2021). Such as, Ni/$ZnAl_2O_4$ combination exhibits superior resistance to carbon deposition and metal sintering. Compared to traditional supports like alumina and silica, which can oxidize Ni during process, zirconia (ZrO_2) offers a significant advantage. ZrO_2 stabilizes Ni particles, leading to a more efficient conversion of methane into fuel. This stability stems from ZrO_2's unique ability to accumulate water, promoting the formation of hydroxyl groups. These hydroxyl groups play a vital role in enhancing the effectiveness of both Steam Reforming of Methane (SRM) and DRM. ZrO_2 and CeO_2 metal oxides emerge as ideal support materials due to their combined benefits. They exhibit a remarkable oxygen storage capacity, exceptional resistance to coking (carbon deposition) and robust redox properties. These attributes result in superior catalytic performance compared to conventional options such as alumina and $MgAl_2O_3$. The Ni-Fe combination shows impressive outcomes, achieving a high methane conversion rate (97.5%) and carbon monoxide selectivity (92.9%) at a temperature of 900 °C (Fakeeha et al., 2022). It has been discovered that basic supports like ZrO_2 accelerate carbon dioxide decomposition and adsorption, creating a durable interaction between metal supports that results in less coke deposition. Additionally, oxides of transition metals form carbonates and oxygen storage capacities (OSCs) that likewise played an important part during DRM reactions. The engineering of support-metal interface is related to a number of O-atoms on metal surfaces. Maximizing the carbon dioxide conversion into carbon monoxide on catalyst surface, efficiently dispersing active phase and avoiding its sintering, a stable, broad surface area must be provided during DRM process (Faria et al., 2014). ZrO_2 is among the most all-around utilized zirconium intensifies in nature. At ambient

pressure, it crystallizes in cubic, monoclinic and tetragonal phases (Chen et al., 2016). Therefore, Ni-based catalyst stability can be increased by using stable support such as zirconia, as it provides an effective pathway to activate CO_2 molecules to generate carbonates in the presence of higher OSCs (Ibrahim et al., 2021).

Zirconia was studied as a support material by Therdthianwong et al. (2008) for DRM catalysts. The review revealed that zirconia significantly upgraded the stability of catalyst with predominant coke hindrance by successfully dissociating oxygen intermediates that in turn, react with carbon species that are produced over surface of metal. ZrO_2 and CeO_2 were metal-supported catalysts synthesized utilizing wet-impregnation approach for DRM process and Abasaeed et al. (2015), investigated calcination temperature impact on these catalysts. Between calcined catalysts, low-temperature-based catalysts exhibited enhanced catalytic activity and yield, in comparison to catalysts that were prepared at higher temperatures. They considered calcination step is a crucial parameter that supports active metal to migrate into porous support by capillary flow. ZrO_2 and CeO_2 were used as support by Yusuf et al. (2020) investigated DRM over nickel-based catalysts. ZrO_2 has been studied as supported by Ibrahim et al. (2021) for DRM process over metal-based catalysts. The results demonstrated that adding support or catalytic promoters to stop creation of carbon has a significant effect on the performance of DRM catalyst. The stability of the DRM catalyst employing ceria and/or zirconia as the supporting material has been studied by Pompeo et al. (2009). According to study, adding support can help to prevent catalyst deactivation by giving the framework a larger commitment to adsorbed oxygen species and encouraging the removal of carbon that has been deposited. Although it has shown promising results in syngas production, topic has received less attention and has not undergone systematic research.

The present research investigates creating a more resilient Ni-based catalyst by focusing on Ni supported by zirconia (Ni-ZrO_2). This is leveraged by zirconia's impressive coking resistance to combat deactivation. By systematically investigating the impact of Ni loading and specific properties of Ni-ZrO_2 interface to achieve optimal performance in terms of hydrogen production, stability and coke resistance. The success of this research could pave the way for efficient syngas production, ultimately contributing to a future powered by clean and sustainable fuels. Optimisation of Ni-ZrO_2 catalysts for DRM could unlock a cleaner, greener future where hydrogen takes centre stage in the fight against climate change.

2. Materials and methods

2.1. Catalyst preparation

The wetness impregnation technique employed in the current work to synthesize catalyst because it produces a catalyst with an even morphology (Selvarajah et al., 2016). Chemicals that are needed include $Ni(NO_3)_2.6H_2O$ and ZrO_2 as metal precursor solutions and catalyst supports, respectively for synthesizing different Ni/ZrO_2 catalysts, both chemicals purchased from Sigma Aldrich having purity 99.9% respectively. A stoichiometric amount of metal precursor solution is combined with a predetermined amount of catalyst support to synthesize various Ni-loadings. For three hours at 25 °C, the resulting mixture is continuously stirred. After finishing three hours of stirring, the mixture is then heated at a rate of 5 K/min for 5 hours while being placed in an oven at 120 °C to finish drying (Abahussain et al., 2024). The calcined catalysts' are named as 5% Ni/ZrO_2, 15% Ni/ZrO_2 and 25% Ni/ZrO_2 respectively. Fig. 1 shows step-wise catalyst preparation through wetness impregnation method.

2.2. Characterization techniques

The textural characteristics of every synthesized catalyst, including pore volume, specific surface area, and pore size, were evaluated using

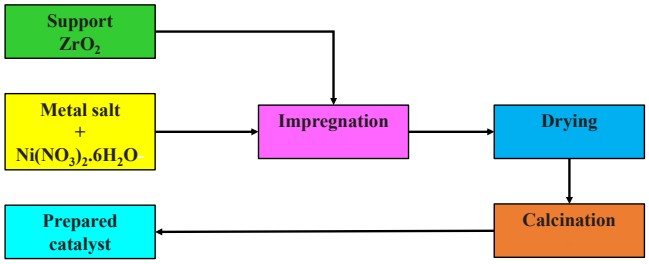

Fig. 1. Process flow diagram for one-step catalyst preparation.

N_2 adsorption-desorption isotherm with liquid nitrogen (-196 °C). The Nova 2200e Quanta chrome surface analyzer based on BET was employed. The substance was initially degassed at 300 °C for three hours in a vacuum before analysis. The crystal structure of the produced catalysts was determined using X-ray diffraction (XRD) method. An advanced diffractometer (Bruker D2-Phaser) was used. The diffractograms were recorded using a source of Cu-K radiation ($\lambda = 1.5418$), which operates between 40 kV and 200 mA and has a detection range of ($2\theta = 10–80°$). FTIR spectra for all synthesized catalysts were obtained using (Shimadzu 8400 FTIR) spectrometer. The spectrometer operated between (400–4000) cm^{-1} range using KBr pellets at room temperature. To determine how much carbon was deposited on the used catalysts, a thermal investigation was conducted using post-responded catalysts. The investigation made use of a Shimadzu TGA thermogravimetric-differential analyzer. The sample (10 mg) was heated to a variety of temperatures at a rate of 25 °C/min and weight variation for each sample was recorded as temperature rose (Abahussain et al., 2024). NOVA NANOSEM 430 and FEI Titan 200, USA were used to obtain SEM-EDS and TEM images, respectively to determine particle morphology and size distribution.

2.3. Experimental setup

Methane was dry reformatted in a fixed bed reactor equipped with a moisture trap and preheater. Feed gases were supplied from compressed cylinders before entering the reactor gases were passed through a silica bed to trap any moisture. The pressure was monitored with the help of a pressure gauge installed before the reactor to maintain atmospheric pressure for reaction. Mass flow controllers regulate flow rate according to the specific requirements for each gas. The catalyst bed within the reactor is positioned just below K-type thermocouple, which is utilized for measuring reactor's temperature. Before entering reactor, the feed gases undergo heating in furnace. The catalyst activity for DRM reaction was evaluated using fixed bed reactor catalysts containing 5, 15, and 25% Ni/ZrO_2, with a feed ratio of 50% methane and 50% carbon dioxide, at atmospheric pressure and elevated temperatures up to 750 °C. To analyze the composition of exhaust gases discharged from reactor, a Gas Chromatograph equipped with a Thermal Conductivity Detector (GC-TCD) is connected to it. The procedure of gas chromatography used helium as a carrier gas. The operating conditions for DRM reaction are described in Table 1. Methane and carbon dioxide conversion was determined via Eq. (5) and Eq. (6) (Azeem et al., 2022) as described below.

Table 1
Reactor operating conditions for catalytic performance evaluation.

Operating conditions	Specifications
H_2 flow rate (reduction)	550 °C, 2 hr (flow rate of 60 mL/min)
Feed	CO_2/CH_4 (equimolar, 99.995%).
Temperature, °C	500–750 and 750 °C for experiments
Pressure	1 atm
Gas hourly space velocity, GHSV	72,000 mL/hr.g_{cat}

$$C_{CH4}\ (\%) = [F_{CH4in} - F_{CH4out}] / F_{CH4in} \times 100 \quad (5)$$

$$C_{CO2}\ (\%) = [F_{CO2in} - F_{CO2out}] / F_{CO2in} \times 100 \quad (6)$$

3. Results and discussion

3.1. Study of synthesized catalysts

Ni-ZrO_2 catalyst is prepared via wetness impregnation method for their potential application in DRM. To understand the structural and textural properties of these catalysts, various characterization techniques were employed, including X-ray diffraction (XRD), scanning electron microscopy (SEM), transmission electron microscopy (TEM), Fourier transform infrared spectroscopy (FTIR), N_2 adsorption-desorption isotherms and activity and stability test. By analyzing the results from these techniques, a comprehensive understanding of catalyst's structure, morphology, surface properties and textural characteristics was established. Ultimately correlating these features with their catalytic performance in DRM.

3.1.1. Textural properties of catalysts

The surface area and pore size distribution of synthesized catalysts were determined by analyzing nitrogen adsorption-desorption isotherms. Table 2 shows that the synthesized catalysts (5, 15 and 25% Ni/ZrO_2) had surface areas and pore volumes of 61, 35.6 and 23.2 m^2/g respectively. These values are identical to those given in the literature (Ibrahim et al., 2022; Ibrahim et al., 2022). Interestingly, a decreasing trend was observed in surface area and pore volume with increasing Ni loading. This decreasing trend can be attributed to several factors, supported by existing literature as (Djinović et al., 2015; Aramouni et al., 2018; Anchieta et al., 2019) demonstrated, that calcination temperature influences catalyst morphology. The decrease in surface area after NiO impregnation indicates successful loading of nickel oxide onto the support. This change could be attributed to the evolution of various gases (H_2O, HNO_3 and O_2) and decomposition of nickel nitrate hexahydrate during calcination process. The absence of distinct NiO peaks in diffraction patterns suggests a potential interaction between NiO and ZrO_2 species in the support. It's also worth noting that weakly bound nickel oxide species are generally easier to reduce but also more susceptible to sintering, leading to the formation of larger particles that can promote carbon formation during the reaction (Sadeq Al-Fatesh et al., 2019). Higher Ni loading might require adjustments to calcination process to prevent pore closure and surface area reduction. Increasing Ni loading often leads to a decline in metal dispersion, as observed by Liu et al. (2018). This can occur due to the formation of larger Ni particles or agglomeration, diminishing the available surface area for adsorption and reaction. Depending on the interaction between Ni and ZrO_2, higher Ni loading could partially block pores within ZrO_2 support, further contributing to the observed decrease in pore volume. According to Fig. 2**(a)**, every catalyst exhibited type-III N_2 adsorption-desorption isotherms with an H_3 type hysteresis loop. However, Fig. 2**(b)** showed that the average pore size distribution of the prepared catalysts ranged from 8.36 to 12.18 nm. Thus, these results proposed that prepared material reflected mesoporous nature (mesoporous $>$ 2 nm and $<$ 50 nm range) (Lanre et al., 2022).

Table 2
Comparison of physical and textural characteristics of catalysts.

Synthesized catalysts	BET surface area (m^2/g)	Pore volume (cm^3/g)	Pore size (nm)
5% Ni/ZrO_2	61.0	0.206	12.18
15% Ni/ZrO_2	35.6	0.128	10.81
25% Ni/ZrO_2	23.2	0.109	8.36

3.1.2. Crystallographic structure of catalysts

To identify crystal phases in the catalyst structure an XRD analysis was performed. The synthesized catalysts' XRD peaks are shown in Fig. 3. The calcined catalysts showed sharp peaks at $2\theta = 37.3°$, 43.3°, 62.9° and 75.3°, confirming the existence of NiO species [JCPDS 22–1189]. The lack of clear diffraction peaks for NiO phase could be due to two factors: (1) nickel oxide particles might be highly dispersed throughout the catalyst and (2) proportion of nickel oxide in overall catalyst structure might be relatively low (Salehi et al., 2024). These observed changes in the catalyst might be due to possibility that ZrO_2 could interact with NiO, forming a mixed oxide containing zirconia and nickel, or the addition of ZrO_2 might act as a diluent, leading to a better dispersion of NiO particles. These well-dispersed particles could be too small for individual detection using employed diffraction technique (Moghaddam et al., 2018).

Additionally, as-prepared catalysts displayed monoclinic and tetragonal zirconia diffraction line features. where the marked peak at $2\theta = 28.4°$ was ascribed as monoclinic phase (111) of ZrO_2 and the major peaks at $2\theta = 30.3°$ and 50.6° related to tetragonal phases (111), (220) [JCPDS 14–0534] (Lanre et al., 2022). However, it is crucial to address the difference in peak intensity observed at 2θ around 25° across samples. This peak corresponds to (111) plane of the monoclinic phase of ZrO_2. Higher Ni content (15% and 25%) might lead to greater dispersion of NiO species on ZrO_2 surface, potentially covering part of monoclinic ZrO_2 phase and reducing the intensity of its related peak. Additionally, the interaction between NiO and ZrO_2 could alter the crystallite size and orientation of monoclinic phase, further affecting peak intensity. Different Ni loadings may induce preferential growth of specific crystal planes in the monoclinic ZrO_2 phase. This could lead to stronger or weaker intensities for (111) peak depending on the dominant plane orientation. A small amount of amorphous phase containing both Ni and Zr could exist in the catalysts, particularly at higher Ni loadings. This amorphous phase wouldn't be captured by XRD, potentially affecting relative intensity of crystalline peaks like monoclinic ZrO_2 (111) peak. The attained patterns were also affirmed in various studies carried out for nickel-zirconia catalysts synthesized through the impregnation method (Singha et al., 2016; Anchieta et al., 2019; Zhang et al., 2019). Moreover, it was revealed by diffraction patterns that like-wise peak intensities appeared for all samples.

3.1.3. Catalytic materials identification

FTIR spectroscopy of fresh Ni supported-ZrO_2 catalysts exhibited in stacked Fig. 4. To determine the types of bands present in synthesized catalysts, analysis is conducted. The band at 1503 cm^{-1} is attributed to $Ni(OH)_2$ species, aligning with observations by Coates (2000). This suggests the presence of residual hydroxyl groups on Ni surface, potentially originating from precursor or interacting with water vapour during sample preparation. The bands at 1363 cm^{-1} and 1624 cm^{-1} correspond to OH bending and stretching modes on ZrO_2 surface, as reported by Reshetenko et al. (2004), Ibrahim et al. (2021). A noticeable increase in the intensity of OH bending vibration peak "around 1624 cm^{-1}" is observed. This observation can be due to hydrogen gas (H_2) being adsorbed onto catalyst surface. This adsorbed hydrogen interacts with surface oxides and water molecules (H_2O) form on catalyst surface. The intensified OH bending vibration peak at "around 1624 cm^{-1}" is likely due to increased presence of these hydroxyl (OH) groups formed during process (Khatri et al., 2021).

These hydroxyl groups play a crucial role in chemisorption phenomena and can influence catalyst activity and stability. Future studies could employ in-situ FTIR techniques under reaction conditions to elucidate dynamic changes in these hydroxyl groups during DRM and their impact on performance. The bands ranging from 500 to 800 cm^{-1} and at 879 cm^{-1} are characteristic of ZrO_2 vibrations, confirming the presence of support material. Further analysis based on specific peak positions and intensities could differentiate between monoclinic and tetragonal phases of ZrO_2, providing insights into crystal structure and

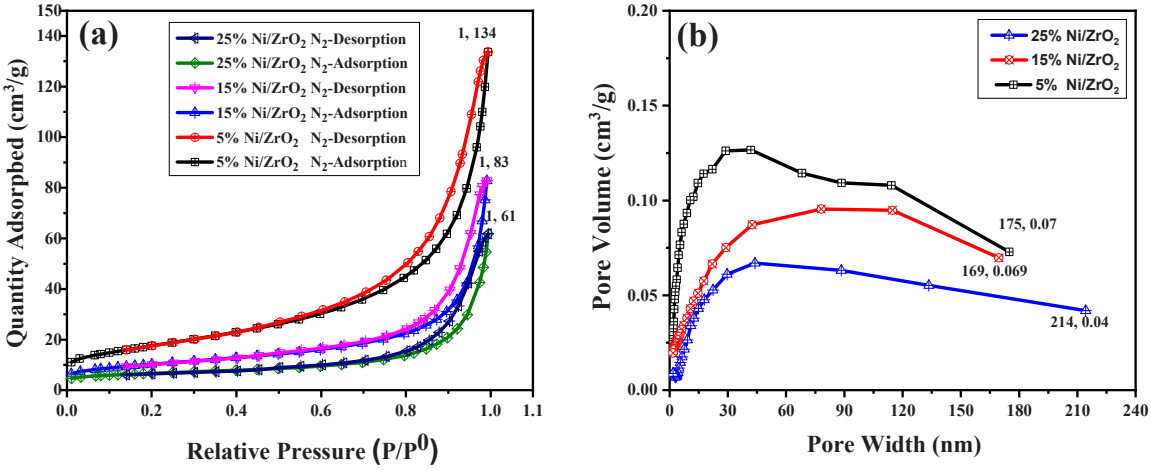

Fig. 2. (a) N_2 adsorption/desorption isotherms and (b) Pore volume distribution of catalysts.

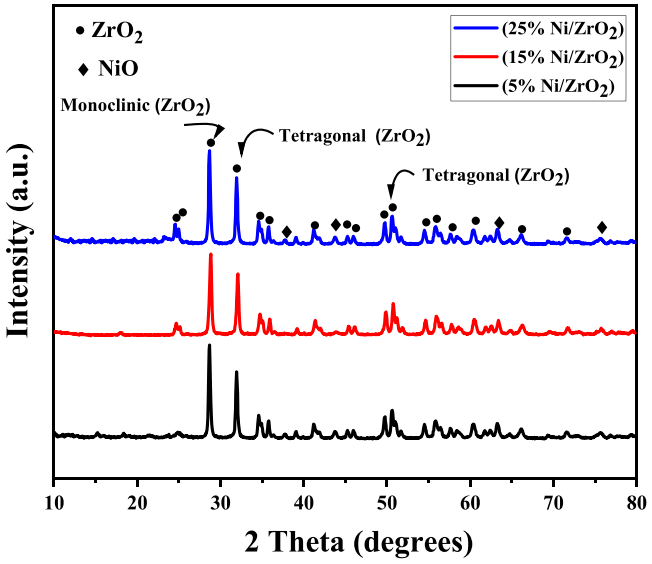

Fig. 3. X-ray diffractogram (XRD) of obtained powder catalysts.

potential influence on support-metal interaction. While overall pattern seems similar across catalysts, a closer look at peak intensities or slight shifts in peak positions might reveal subtle differences related to Ni loading and its influence on surface properties. Comparing these observations with recent literature (Ibrahim et al., 2022; Ibrahim et al., 2022), could shed light on how Ni loading affects the abundance and interaction of various surface species like hydroxyl groups and their potential impact on catalytic behaviour.

3.1.4. *Catalysts surface topography*

SEM-EDS study was conducted to examine the surface morphology of all synthesized catalysts, the attained results depicted qualitatively similar nano-scale topography. Fig. 5 and Fig. 6 show SEM images along with the best EDS spectra respectively. The resulting SEM images indicated that for all catalysts, a homogeneous spherical distribution is visible as the catalyst surface that is covered with bunches of particles with various sizes ranging from (10–40) nm that are made of ZrO_2 as seen in Fig. 5**(a, b, c)**. This supports enhancement of Zr on the surface that is firmly accepted to be ZrO_2 out of bulk (Walker et al., 2012; Goula et al., 2017). EDX images are also re-endorsed for the zirconia-rich regions with the clusters. The recorded peaks confirmed the attendance of Ni, Zr and O elements from EDS spectra (Liu et al., 2018) as shown in Fig. 6**(a, b)**. EDS results established that nickel metal loading attained around the calculated values for best two samples (Goula et al., 2017; Liu et al., 2018).

3.2. *Catalyst activity and stability performance*

The conversion of carbon dioxide and methane over a variety of Ni/ZrO_2 catalysts (5, 15 and 25 wt%) at temperatures between (550 and 750 °C) was used to determine the catalytic activity. The reaction conditions (GHSV = 72,000 mL/h.g_{cat}, P = 1 atm) were kept constant during the experiment for each catalyst. Fig. 7**(a, b)** showed activity results for the conversion of methane and carbon dioxide for synthesized catalysts respectively. At a reaction temperature of 750 °C, 15% Ni/ZrO_2 catalyst demonstrated enhanced conversion rates for CH_4 and CO_2. At 750 °C, 5% Ni/ZrO_2 and 25% Ni/ZrO_2 catalysts demonstrated lower CH_4 and CO_2 conversion values than 15% Ni/ZrO_2 showed. CH_4 conversion was accomplished at 44.5, 62.9 and 59.9% using catalysts of 5% Ni-ZrO_2, 15% Ni-ZrO_2 and 25% Ni-ZrO_2, correspondingly. While 5% Ni-ZrO_2 achieved CO_2 conversion, 15% Ni-ZrO_2 and 25% Ni-ZrO_2 catalysts achieved CO_2 conversion at rates of 49.9, 64.9 and 58%, respectively. It is discovered that the conversion of carbon dioxide is larger than the conversion of CH_4 as a result of influence of reverse water-gas shift reaction ($H_2 + CO_2 \leftrightarrow H_2O + CO$). In comparison to 15% Ni/ZrO_2 catalytic activity, the catalyst with increased Ni loading displayed reduced activity. Particles that have gathered on the surface might explain why catalyst activity decreases when nickel concentration increases and vice versa. When the reaction first began, 25% Ni-ZrO_2 catalyst was significantly more active up to a temperature of around 680 °C but as time went on, the carbon buildup on catalyst's active sites caused its activity to progressively decline. Nickel particle agglomeration was visible in SEM images of 25% Ni/ZrO_2, which may be a primary factor in the catalyst's decreased activity.

The catalyst stability for all Ni/ZrO_2 based-catalysts investigated for DRM process at given reaction conditions (Constant reaction temperature= 750 °C) for 450 minutes and outcomes are shown in Fig. 7 **(c, d)**. The most stable catalyst for converting methane and carbon dioxide was 15% Ni-ZrO_2. When the response first began, methane conversion for 15% Ni-ZrO_2 was 63.42% with time on stream at stable 750 °C, its CH_4 conversion only decreased 5.35% and maintained at 57.08% towards the end of reaction. Similarly, CO_2 conversion of 15% Ni-ZrO_2 catalyst at the start was 64.92%, showed only 6.72% decline at the end of reaction and maintained at 58.2%, respectively at stable 750 °C. Methane and carbon dioxide conversion were lower with 5% Ni/ZrO_2 and 25% Ni/ZrO_2 catalysts compared to 15% Ni/ZrO_2 (41.9, 44.9 and 51.2%) respectively. The increased stability can be explained by better coke resistance and sintering of metal particles. Because deposition of coke

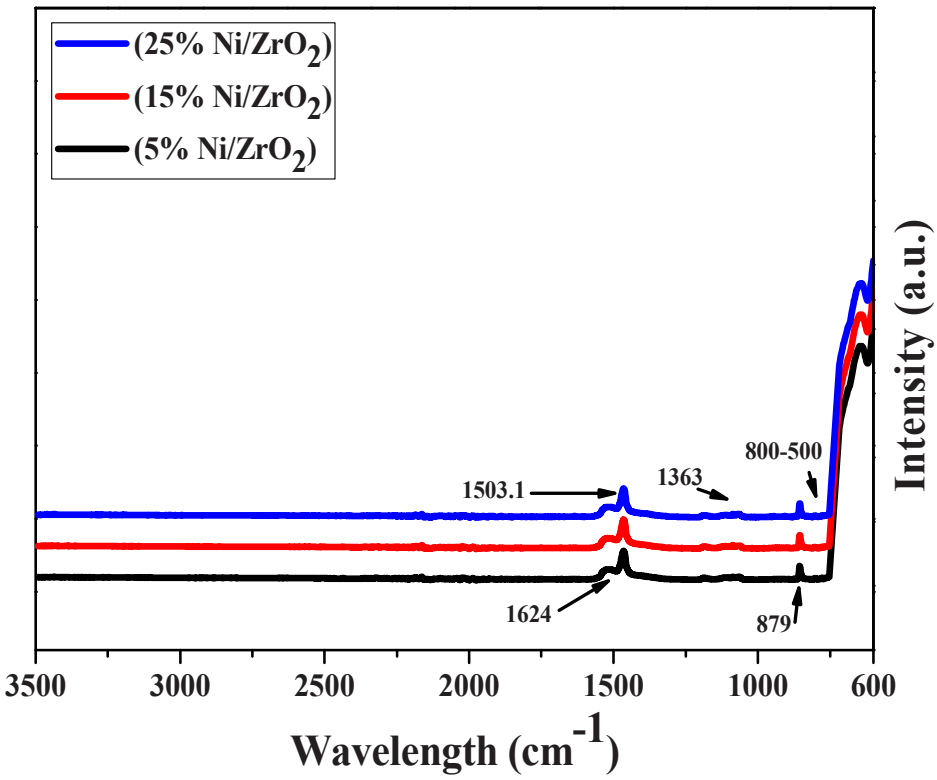

Fig. 4. FTIR spectroscopy of fresh catalysts; 5% Ni/ZrO_2 (black), 15% Ni/ZrO_2 (red), 25% Ni /ZrO_2 (blue).

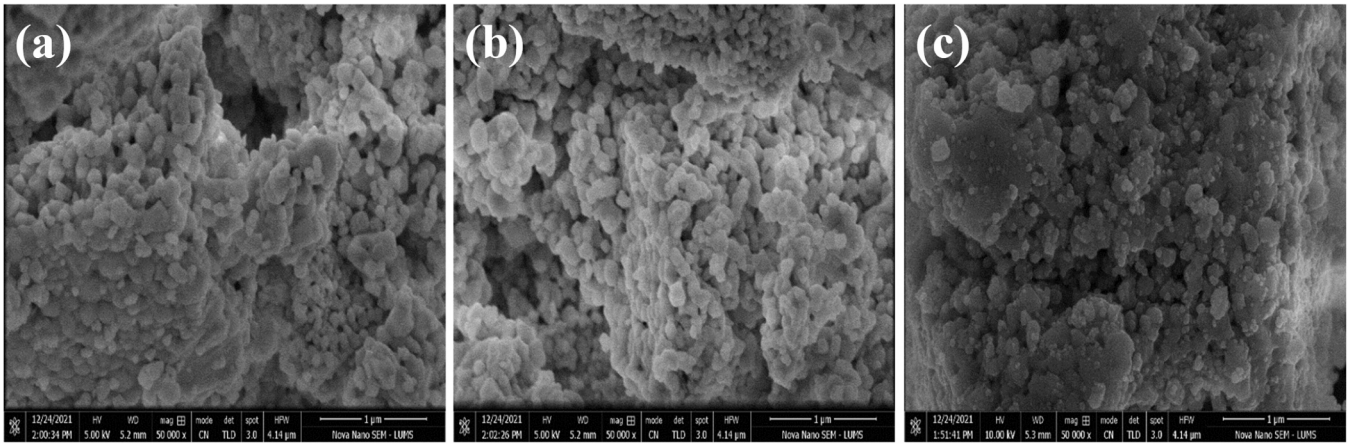

Fig. 5. SEM images of synthesized Ni–ZrO_2 catalysts; (a) 5%, (b) 15% and (c) 25% Ni-metal doping.

ultimately reduces catalyst stability due to blockage of active Ni-species on the catalyst surface (Che and Bennett, 1989; Ibrahim et al., 2021).

Similar to previous studies (Horlyck et al., 2018; Anzures et al., 2021), our research suggests that specific surface area of catalyst plays a crucial role in methane conversion during DRM. A lower specific surface area can limit conversion efficiency. A well-known challenge in DRM is catalyst deactivation caused by carbon deposition on the catalyst surface. This phenomenon is confirmed by Scanning Electron Microscope (SEM) images in Fig. 10. This catalyst exhibits a significant amount of filamentous carbon deposition Fig. 10**(a, c)**, which aligns with observations by Sokolov et al. (2017). Their study reported extensive formation of large carbon filaments, leading to a gradual and continuous deactivation of 5%, 25% Ni/ZrO_2 catalyst due to blocked active sites. This aligns with findings reported in the literature (Ali et al., 2020). The impact of ZrO_2 content on carbon deposition is evident. 15 wt% Ni/ZrO_2 catalyst shows minimal carbon deposition, suggesting better resistance compared to 5 and 25 wt% Ni/ZrO_2.

Ibrahim et al. (2021) studied DRM reaction using Ni-ZrO_2 catalysts and reported 54% methane conversion at reaction a condition of (GHSV of 42000 mL/h·g_{cat} and 700 °C). Prior literature addressed that the conversion should be higher at lower GHSV values, establishing higher contact time and vice versa. Fakeeha et al. (2013), Fakeeha et al. (2021) stated 76% conversion of methane at lower GHSV of 3600 mL/h·gcat at 700 °C over Ni/H-ZSM-5. Pan et al. (2020) stated 69% CH_4 conversion 10% Ni/Al_2O_3 at GHSV of 24,000 mL/h·g_{cat} and 700 °C. In their study of DRM utilizing MgO-promoted Ni/Al_2O_3, Jin et al. (2021) found that 36% of methane was converted at 800 °C with a reduced GHSV of 6, 000 mL/h.g_{cat}. At higher GHSV of 86000 mL/h.g_{ca}t and 760 °C over Ni-MgO, Zhang et al. (2020) found a 70% methane conversion. In the present study, methane's highest conversion of 62.9% is obtained

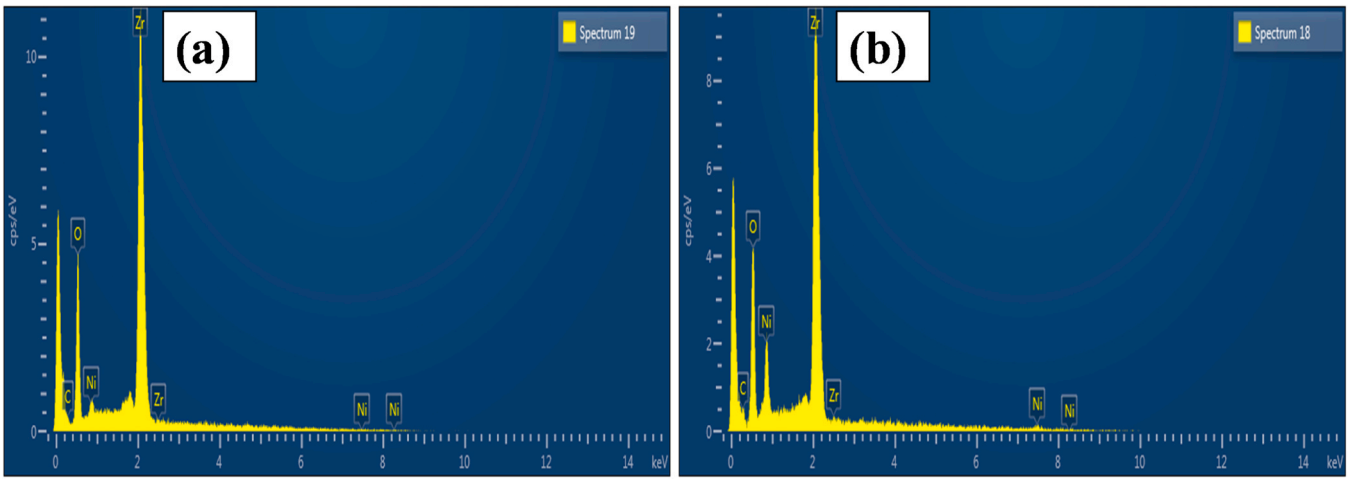

Fig. 6. Energy dispersive X-ray analysis (EDX) spectrum of fresh; (a) 5% Ni/ZrO_2 and (b) 15% Ni/ZrO_2 catalyst.

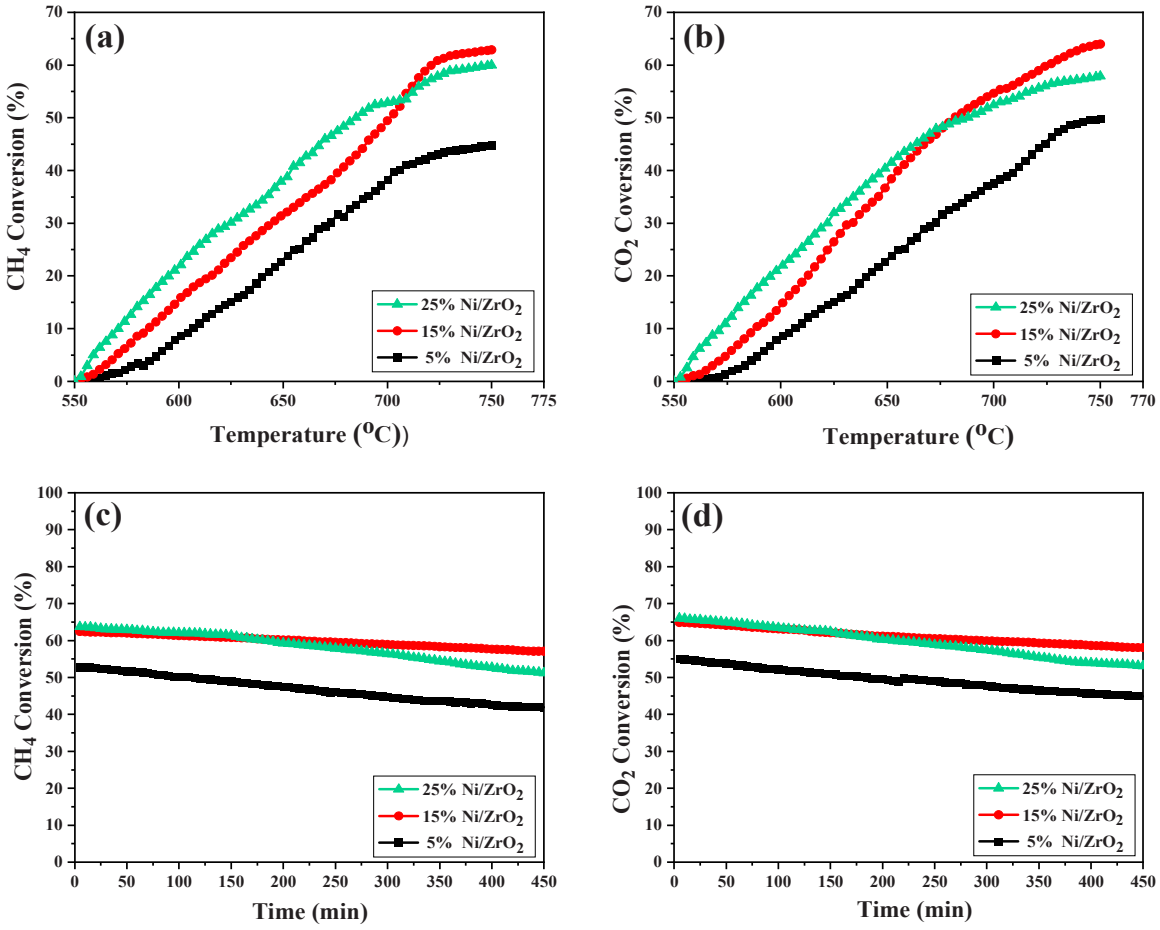

Fig. 7. Activity of all catalysts; (a) CH_4 conversion, (b) CO_2 conversion as a function of temperature and stability of catalysts, (c) CH_4 conversion and (d) CO_2 conversion as a function of time.

relatively at higher GHSV, those are similar to conversions mentioned in the literature. The performance of nickel-based DRM catalyst is compared with cited literature in Table 3 using varied GHSV and temperature values. In comparison to other catalysts used under specified reaction conditions, it may be seen that this one provides the maximum yield for DRM process.

3.3. Characterization of spent catalysts

3.3.1. Catalysts microscopic analysis

After assessing structural and textural properties of the synthesized Ni-ZrO_2 catalysts, it is essential to comprehend how these attributes influence their performance under DRM conditions. This section concentrates on examination of spent catalysts following DRM reaction, employing a range of characterization techniques similar to those used

Table 3
Comparison of Ni-based catalysts reported in the literature and obtained in this work for DRM reaction.

CH_4 Conversion (%)	GHSV (mL/h. g_{cat})	Temperature (^oC)	Reference
36	6000	800	(Jin et al., 2021)
53	42000	700	(Al-Mubaddel et al., 2021)
66	8000	700	(Al-Fatesh et al., 2019)
50	48000	800	(Yan et al., 2019)
85	39000	800	(Al-Fatesh et al., 2021)
67	42000	700	(Ibrahim et al., 2022)
38	3000	850	(Mesrar et al., 2018)
54	42000	700	(Ibrahim et al., 2021)
41	24000	700	(Pan et al., 2020)
83	24000	850	(Leba and Yıldırım, 2020)
87	48000	700	(Wang et al., 2022)
72	15000	800	(Setiabudi et al., 2017)
69	30000	800	(Hambali et al., 2020)
70	86000	760	(Zhang et al., 2020)
21	60000	600	(Wang et al., 2022)
79	60000	700	(Mesrar et al., 2018)
45	13000	800	(Ibrahim et al., 2019)
67	42000	700	(Ibrahim et al., 2022)
62.9	**72000**	**750**	**This Work**

for fresh catalysts. The changes in morphology, composition and surface properties of used catalysts were studied to gain insights into interactions between catalyst materials and reactants during DRM process. Such insights could help elucidate potential deactivation mechanisms, identify factors influencing catalyst stability and ultimately guide further optimization strategies for improved DRM performance. TEM analysis of each used Ni-ZrO_2 catalyst was displayed in Fig. 8**(a, b, c)**. Following reaction, Ni-particles on the support were uniformly distributed, as seen in TEM topographic image of 15% Ni-ZrO_2 catalyst that is also detailed in published studies (Ibrahim et al., 2019). Additionally, a 15% Ni-ZrO_2 catalyst showed that whisker carbon does not emerge (Zhang et al., 2021). After stability testing, 5% and 25% Ni-ZrO_2 revealed catalyst particle sintering. TEM images in Fig. 8 **(a, c)** indicate that deactivation of nickel might occur through sintering of metallic nickel particles. This observation aligns with the visual evidence. Furthermore, an accumulation of carbon nanotubes was observed on both catalysts (5% and 25% Ni/ZrO_2), with a more extensive presence on the sample. This suggests that the method of catalyst preparation might influence extent of carbon deposition. A study by (Yahi et al., 2015) revealed that carbon species formed on Ni-ZrO_2 catalysts prepared by wetness impregnation primarily exist in oxidized forms. These oxidized carbon forms are known to be less reactive towards gasification, making them more persistent. The accumulation of such carbon can cover active nickel sites, hindering their catalytic activity and leading to rapid deactivation. The higher Ni loading also influenced sintering susceptibility. The observed sintering and agglomeration might be due to large particle size and loss of distinct boundaries that resulted in the reduction of active surface area and hindered reactant access (Zhang et al., 2022). Therefore, 15% Ni-ZrO_2 demonstrated great resistance to metal sintering and as a result, enhanced catalytic activity can be linked to this material's resistance to particle agglomeration that is precisely linked to better metal-support interaction. However, higher heat sintering of the particles made the 5% and 25% Ni/ZrO_2 catalysts more susceptible to loss of catalytic activity.

3.3.2. *Temperature dependent weight loss analysis*

The weight loss of all spent catalysts was estimated through TGA study as displayed in Fig. 9. In TGA examination, catalysts' little weight loss was seen between (600 and 900) °C. Each TGA profile showed

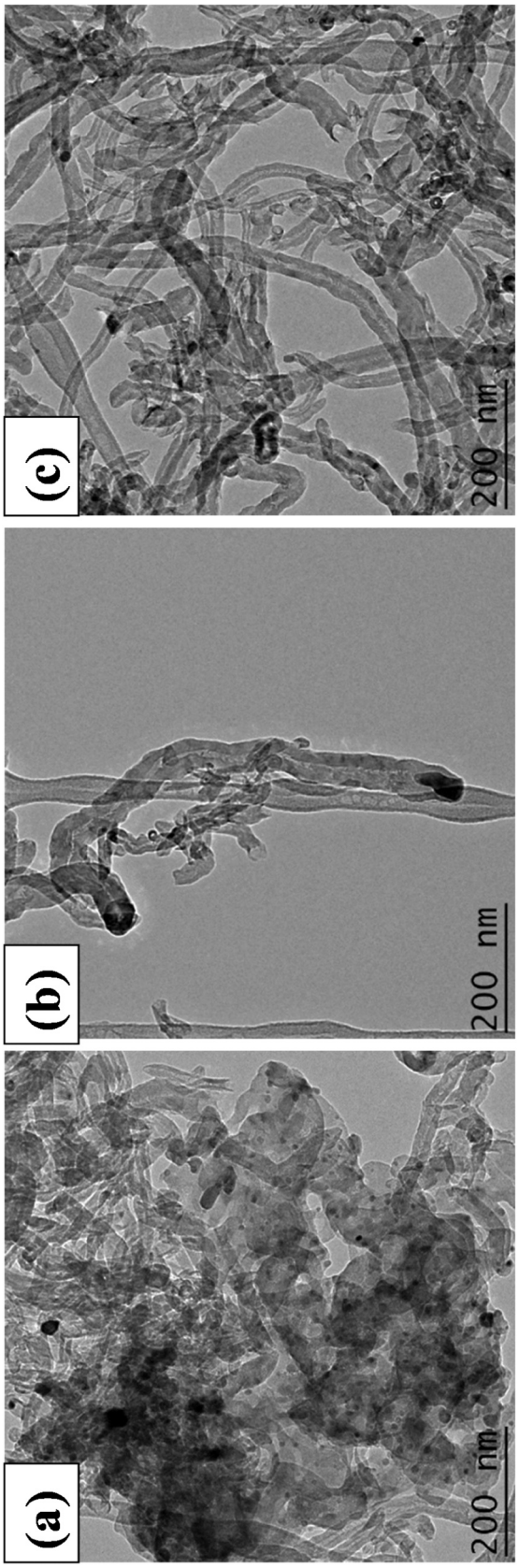

Fig. 8. TEM images of spent catalyst; (a) 5% Ni/ZrO_2, (b) 15% Ni/ZrO_2 and (c) 25% Ni/ZrO_2.

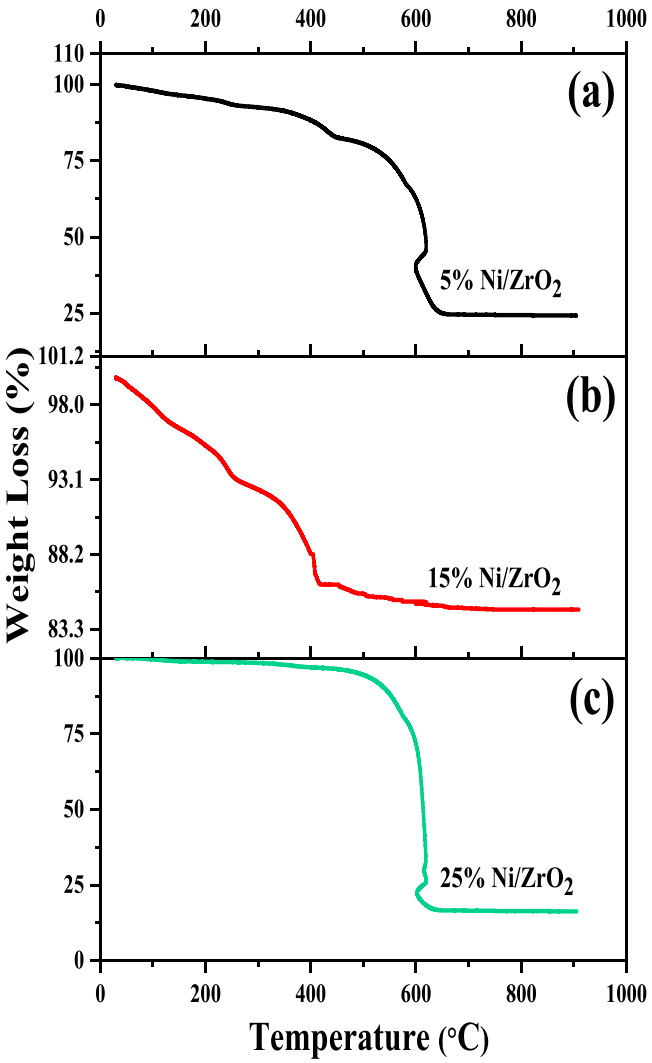

Fig. 9. Thermogravimetric analysis (TGA) of spent catalysts.

catalyst's thermal stability at the corresponding temperature. However, depending on the species present on the sample surface, TGA profile revealed three zones for each catalyst weight reduction. The first zone of weight loss occurred between (50–200 °C), associated with poorly absorbed water contents. The second region (200–500 °C) displayed Ni $(OH)_2$ disintegration or production of surface carbon coke. Temperatures above 500 °C led to weight loss in the third region, reflecting different types of carbon species such as NiC_x, which is quite similar to already reported trends in published literature (Singha et al., 2016; Anchieta et al., 2019). TGA profile of 5% Ni-ZrO_2 test showed a complete 83.73% weight reduction at (50–900) °C as demonstrated in Fig. 9 **(a)**. While 15% Ni-ZrO_2 TGA profile at temperatures between (50–900 °C) revealed a total weight loss of 15.42% as shown in Fig. 9**(b)**. As a consequence of absorbed H_2O molecules and Ni $(OH)_2$ breakdown, the primary weight loss (12.62 wt%) of 15% Ni-ZrO_2 sample took place at (50–390 °C) temperature range, or generation of surface carbon coke. At temperatures between (390 and 900 °C), a second weight loss (2.80 wt %) of 15% Ni-ZrO_2 was observed due to carbon that had been deposited and was escaping as carbon monoxide or carbon dioxide.

Conversely, the catalyst with 15% Ni/ZrO_2 showed minimal weight loss suggesting suppressed carbon deposition. This observation aligns with overall activity of catalysts. Generally, higher reaction activity can lead to a greater degree of carbon formation. Fig. 9**(c)** displayed a total weight loss of around 75.79% at (50–900) °C with a 25% Ni-ZrO_2 catalyst. Above all, 5% Ni/ZrO_2 and 25% Ni/ZrO_2 samples exhibited rapid deactivation profiles, which is owing to carbon deposition on spent catalysts surface in comparison to 15% Ni/ZrO_2 sample that attained higher coke resistance. One possible explanation for this stabilizing effect is the potential for a high loading to excessively cover the active nickel sites. This could reduce the reactivity of nickel and consequently decrease carbon deposition. The excessive coke formation in 5% and 25% Ni/ZrO_2 catalysts can lead to rapid deactivation. Higher Ni loading might initially increase coke formation due to more available active sites. Yet, achieving optimal dispersion and fostering strong metal-support interaction can help mitigate and restrict carbon deposition (Zhang et al., 2022).

3.3.3. *Spent samples surface topography*

The observed filamentous carbon on 5% and 25% Ni/ZrO_2 catalysts significantly hinders their activity and stability compared to 15% Ni/ZrO_2 catalyst. The filamentous carbon entangles catalyst surface and physically blocks vital Ni sites. The intricate network of carbon filaments acts as a barrier, hindering the transport of reactant molecules to active sites and product molecules away from them. This further reduces reaction rates and overall activity. This carbon presence can alter catalyst's electronic and geometric properties, potentially affecting reactant adsorption and activation, leading to decreased activity (Wang et al., 2022; Wang et al., 2022). However, Fig. 10**(a, c)** also demonstrates considerable particle agglomeration. This causes stability and activity of catalyst to decline, which accelerates the catalyst's surface deactivation process (Al-Fatesh et al., 2019). The findings from morphology analysis of spent catalysts (potentially referring to techniques like SEM or TEM) corroborate the results obtained from thermogravimetric analysis (TGA), which likely indicated the presence of carbon deposition. The absence of extensive filamentous carbon in 15% Ni/ZrO_2 catalyst minimizes these negative impacts. The characterization results, activity and stability tests on 15% Ni/ZrO_2 catalyst show superior outcomes. This can be attributed to striking a balance between active sites and coke resistance, hindering carbon precursor formation and promoting coke desorption and inhibiting coke adhesion or promoting CO_2 desorption.

4. Conclusion

DRM presents a compelling solution for mitigating greenhouse gas emissions by transforming CH_4 and CO_2 into valuable renewable fuels. However, widespread adoption depends on overcoming catalyst deactivation induced by carbon deposition on the catalyst surface. This study explores Ni-supported ZrO_2 catalysts (5, 15 and 25 wt% Ni) potential to address said challenge. Amongst the investigated catalysts, 15% Ni/ZrO_2 catalyst proved superior methane and CO_2 conversions exceeding 65% values during a time-on screen for 450 minutes for DRM reaction. This remarkable performance arises from optimized metal-support interaction, demonstrated by TGA and TEM analysis revealing the absence of graphitic carbon on the spent catalyst's surface. In contrast, other variations of Ni loadings (5% and 25%) exhibited particle agglomeration, surface sintering, filamentous carbon deposition, and higher coke formation, leading to activity decline at elevated temperatures. This study highlights the pivotal role of tuning Ni loading in Ni-ZrO_2 catalysts. 15% Ni/ZrO_2 system achieves a unique balance between catalytic activity and coke resistance, offering a promising solution for efficient and sustainable production of green hydrogen. Notably, improved coke resistance stems from synergetic effect between Ni-metal and ZrO_2 support, opening avenues for further exploring metal-support interactions in catalyst design. The impregnation method utilized in this study likely facilitated uniform dispersion of nickel on zirconia support, thereby ensuring active nickel phase remains readily available for DRM reaction. Additionally, the study sheds light on several secondary processes occurring during DRM, including gasification of carbon (C) and carbon monoxide (CO), thermal decomposition of methane (CH_4) and carbon dioxide (CO_2), as well as water-gas shift (WGS) and reverse water-gas shift (RWGS) reactions. Based on the findings, incorporating

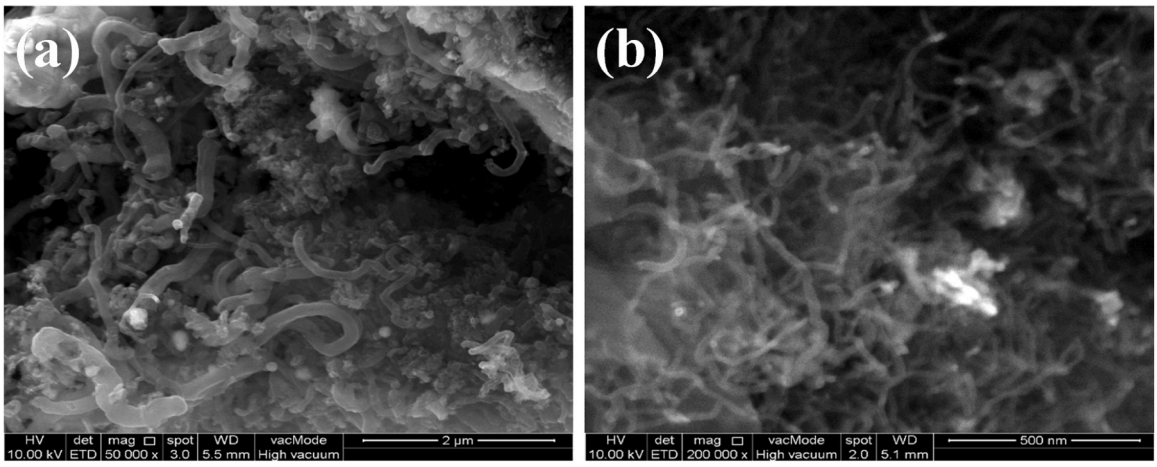

Fig. 10. SEM micrographs of spent catalysts; (a) 5% Ni/ZrO_2 and (b) 25% Ni/ZrO_2.

15 wt% Ni/ZrO_2 appears to be the optimal approach for stabilizing catalysts under these specific DRM reaction conditions. This optimized catalyst demonstrates exceptional resistance against the formation of filamentous coke, a major deactivation factor in DRM. By optimizing Ni-ZrO_2 catalysts for DRM, this research contributes significantly to efficient conversion of methane into syngas paving the way for clean fuel generation, reducing reliance on fossil fuels and mitigating climate change impact. Enhanced catalyst stability ensures longer operational life and minimizes catalyst replacement costs, making DRM more attractive for industrial applications. Insights gained from this study inform the development of new catalysts with tailored properties for diverse energy conversion processes. Future research can delve deeper into understanding the specific mechanisms governing synergetic effect in 15% Ni/ZrO_2 catalyst and explore strategies for further enhancing stability and activity. Additionally, scaling up catalyst synthesis and testing its performance under realistic industrial conditions will be crucial for realizing its full potential in large-scale hydrogen production via DRM.

CRediT authorship contribution statement

Subhan Azeem: Conceptualization, Formal analysis, Investigation, Writing – original draft. **Muddasar Safdar:** Data curation, Resources, Validation, Writing – original draft. **Bohong Wang:** Funding acquisition, Validation, Writing – review & editing. **Sabah Ansar:** Funding acquisition, Writing – review & editing. **Rabya Aslam:** Conceptualization, Project administration, Supervision, Writing – original draft. **Imane Ziani:** Resources, Software, Writing – review & editing. **Farooq Sher:** Funding acquisition, Project administration, Supervision, Writing – review & editing.

Declaration of Competing Interest

The authors declare that they have no known competing financial interests or personal relationships that could have appeared to influence the work reported in this paper.

Acknowledgement

The authors are grateful for financial support from the International Society of Engineering Science and Technology (ISEST) UK. The authors thank the Researchers Supporting Project number (RSP2024R169), King Saud University, Riyadh, Saudi Arabia for the financial support.

References

Abahussain, A.A., Al-Fatesh, A.S., Singh, S.K., Almutairi, G., Fakeeha, A.H., Ibrahim, A. A., Abasaeed, A.E., Frusteri, L., Labhasetwar, N.K., 2024. Cs promoted Ni/ZrO_2-Al_2O_3 catalysts for dry reforming of methane: promotional effects of Cs for enhanced catalytic activity and stability. Arab. J. Chem. 17 (2), 105564.

Abasaeed, A.E., Al-Fatesh, A.S., Naeem, M.A., Ibrahim, A.A., Fakeeha, A.H., 2015. Catalytic performance of CeO_2 and ZrO_2 supported Co catalysts for hydrogen production via dry reforming of methane. Int. J. Hydrog. Energy 40 (21), 6818–6826.

Al-Fatesh, A.S., Abu-Dahrieh, J.K., Atia, H., Armbruster, U., Ibrahim, A.A., Khan, W.U., Abasaeed, A.E., Fakeeha, A.H., 2019. Effect of pre-treatment and calcination temperature on Al_2O_3-ZrO_2 supported Ni-Co catalysts for dry reforming of methane. Int. J. Hydrog. Energy 44 (39), 21546–21558.

Al-Fatesh, A.S., Arafat, Y., Ibrahim, A.A., Kasim, S.O., Alharthi, A., Fakeeha, A.H., Abasaeed, A.E., Bonura, G., Frusteri, F., 2019. Catalytic behaviour of Ce-doped Ni systems supported on stabilized zirconia under dry reforming conditions. Catalysts 9 (5), 473.

Al-Fatesh, A.S., Fakeeha, A.H., Ibrahim, A.A., Abasaeed, A.E., 2021. Ni supported on La_2O_3+ ZrO_2 for dry reforming of methane: the impact of surface adsorbed oxygen species. Int. J. Hydrog. Energy 46 (5), 3780–3788.

Al-Fatesh, A.S., Kumar, R., Kasim, S.O., Ibrahim, A.A., Fakeeha, A.H., Abasaeed, A.E., Atia, H., Armbruster, U., Kreyenschulte, C., Lund, H., 2021. Effect of cerium promoters on an MCM-41-supported nickel catalyst in dry reforming of methane. Ind. Eng. Chem. Res. 61 (1), 164–174.

Ali, S., Khader, M.M., Almarri, M.J., Abdelmoneim, A.G., 2020. Ni-based nano-catalysts for the dry reforming of methane. Catal. Today 343, 26–37.

Al-Mubaddel, F.S., Kumar, R., Sofiu, M.L., Frusteri, F., Ibrahim, A.A., Srivastava, V.K., Kasim, S.O., Fakeeha, A.H., Abasaeed, A.E., Osman, A.I., 2021. Optimizing acido-basic profile of support in Ni supported La_2O_3+ Al_2O_3 catalyst for dry reforming of methane. Int. J. Hydrog. Energy 46 (27), 14225–14235.

Anchieta, C.G., Assaf, E.M., Assaf, J.M., 2019. Effect of ionic liquid in Ni/ZrO_2 catalysts applied to syngas production by methane tri-reforming. Int. J. Hydrog. Energy 44 (18), 9316–9327.

Anzures, F.M., Hernández, P.S., Galicia, G.M., Martínez, A.G., Morales, F.T., Romo, M.A. R., Hernández, R.P., 2021. Synthetic gas production by dry reforming of methane over Ni/Al_2O_3–ZrO_2 catalysts: high H_2/CO ratio. Int. J. Hydrog. Energy 46 (51), 26224–26233.

Aramouni, N.A.K., Touma, J.G., Tarboush, B.A., Zeaiter, J., Ahmad, M.N., 2018. Catalyst design for dry reforming of methane: analysis review. Renew. Sustain. Energy Rev. 82, 2570–2585.

Azeem, S., Aslam, R., Saleem, M., 2022. Dry reforming of methane with mesoporous Ni/ZrO 2 catalyst. Int. J. Chem. Eng. **2022**.

Bian, Z., Kawi, S., 2018. Sandwich-like silica@ Ni@ silica multicore–shell catalyst for the low-temperature dry reforming of methane: Confinement effect against carbon formation. ChemCatChem 10 (1), 320–328.

Che, M., Bennett, C.O., 1989. The Influence of Particle Size on the Catalytic Properties of Supported Metals. In: Eley, D.D., Pines, H., Weisz, P.B. (Eds.), Advances in Catalysis, **36**. Academic Press, pp. 55–172.

Chen, L., Qi, Z., Zhang, S., Su, J., Somorjai, G.A., 2020. Catalytic hydrogen production from methane: a review on recent progress and prospect. Catalysts 10 (8), 858.

Chen, A., Zhou, Y., Miao, S., Li, Y., Shen, W., 2016. Assembly of monoclinic ZrO_2 nanorods: formation mechanism and crystal phase control. CrystEngComm 18 (4), 580–587.

Coates, J. (2000). Interpretation of infrared spectra, a practical approach.

Davies, W., S. Babamohammadi, Y. Yan, P. Clough and S. Masoudi Soltani (2024). Exergy Analysis in Intensification of Sorption-enhanced Steam Methane Reforming for Clean Hydrogen Production: Comparative Study and Efficiency Optimisation.

Djinović, P., Črnivec, I.G.O., Pintar, A., 2015. Biogas to syngas conversion without carbonaceous deposits via the dry reforming reaction using transition metal catalysts. Catal. Today 253, 155–162.
Fakeeha, A.H., Al Fatesh, A.S., Ibrahim, A.A., Kurdi, A.N., Abasaeed, A.E., 2021. Yttria modified ZrO_2 supported Ni catalysts for CO_2 reforming of methane: the role of Ce promoter. ACS Omega 6 (2), 1280–1288.
Fakeeha, A.H., Al-Fatesh, A.S., Abasaeed, A.E., 2013. Stabilities of zeolite-supported Ni catalysts for dry reforming of methane. Chin. J. Catal. 34 (4), 764–768.
Fakeeha, A.H., Kurdi, A., Al-Baqmaa, Y.A., Ibrahim, A.A., Abasaeed, A.E., Al-Fatesh, A.S., 2022. "Performance study of methane dry reforming on Ni/ZrO_2 catalyst". Energies 15 (10), 3841.
Faria, E., Neto, R., Colman, R., Noronha, F., 2014. Hydrogen production through CO_2 reforming of methane over Ni/$CeZrO_2$/Al_2O_3 catalysts. Catal. Today 228, 138–144.
Gao, X., Ashok, J., Kawi, S., 2020. Smart designs of anti-coking and anti-sintering Ni-based catalysts for dry reforming of methane: a recent review. Reactions 1 (2), 162–194.
Goula, M., Charisiou, N., Siakavelas, G., Tzounis, L., Tsiaoussis, I., Panagiotopoulou, P., Goula, G., Yentekakis, I., 2017. Syngas production via the biogas dry reforming reaction over Ni supported on zirconia modified with CeO_2 or La_2O_3 catalysts. Int. J. Hydrog. Energy 42 (19), 13724–13740.
Goula, M.A., Charisiou, N.D., Siakavelas, G., Tzounis, L., Tsiaoussis, I., Panagiotopoulou, P., Goula, G., Yentekakis, I.V., 2017. Syngas production via the biogas dry reforming reaction over Ni supported on zirconia modified with CeO_2 or La_2O_3 catalysts. Int. J. Hydrog. Energy 42 (19), 13724–13740.
Guharoy, U., Reina, T.R., Liu, J., Sun, Q., Gu, S., Cai, Q., 2021. A theoretical overview on the prevention of coking in dry reforming of methane using non-precious transition metal catalysts. J. CO_2 Util. 53, 101728.
Guo, S., Sun, Y., Zhang, Y., Zhang, C., Li, Y., Bai, J., 2024. Bimetallic Nickel-Cobalt catalysts and their application in dry reforming reaction of methane. Fuel 358, 130290.
Hambali, H.U., Jalil, A.A., Abdulrasheed, A.A., Siang, T.J., Vo, D.-V.N., 2020. Enhanced dry reforming of methane over mesostructured fibrous Ni/MFI zeolite: Influence of preparation methods. J. Energy Inst. 93 (4), 1535–1543.
Horlyck, J., Lewis, S., Amal, R., Scott, J., 2018. The impact of La doping on dry reforming Ni-based catalysts loaded on FSP-alumina. Top. Catal. 61, 1842–1855.
Ibrahim, A.A., Al-Fatesh, A.S., Khan, W.U., Kasim, S.O., Abasaeed, A.E., Fakeeha, A.H., Bonura, G., Frusteri, F., 2019. Enhanced coke suppression by using phosphate-zirconia supported nickel catalysts under dry methane reforming conditions. Int. J. Hydrog. Energy 44 (51), 27784–27794.
Ibrahim, A.A., Fakeeha, A.H., Abasaeed, A.E., Al-Fatesh, A.S., 2021. Dry reforming of methane using Ni catalyst supported on ZrO_2: the effect of different sources of Zirconia. Catalysts 11 (7), 827.
Ibrahim, A.A., Fakeeha, A.H., Lanre, M.S., Al-Awadi, A.S., Alreshaidan, S.B., Albaqmaa, Y.A., Adil, S.F., Al-Zahrani, A.A., Abasaeed, A.E., Al-Fatesh, A.S., 2022. The effect of calcination temperature on various sources of ZrO_2 supported Ni catalyst for dry reforming of methane. Catalysts 12 (4), 361.
Ibrahim, A.A., Kasim, S.O., Fakeeha, A.H., Lanre, M.S., Abasaeed, A.E., Abu-Dahrieh, J. K., Al-Fatesh, A.S., 2022. Dry reforming of methane with Ni supported on mechanically mixed Yttria-Zirconia support. Catal. Lett. 152 (12), 3632–3641.
Jahangiri, H., Lappas, A.A., Ouadi, M., Heracleous, E., 2023. Production of Biofuels via Fischer-Tropsch Synthesis: Biomass-to-Liquids. Handbook of Biofuels Production. Elsevier, pp. 449–509.
Jin, B., Li, S., Liang, X., 2021. Enhanced activity and stability of MgO-promoted Ni/Al_2O_3 catalyst for dry reforming of methane: role of MgO. Fuel 284, 119082.
Khatri, J., Fakeeha, A.H., Kasim, S.O., Lanre, M.S., Abasaeed, A.E., Ibrahim, A.A., Kumar, R., Al-Fatesh, A.S., 2021. Ceria promoted phosphate-zirconia supported Ni catalyst for hydrogen rich syngas production through dry reforming of methane. Int. J. Energy Res. 45 (13), 19289–19302.
Kiani, P., Meshksar, M., Rahimpour, M.R., 2023. Biogas reforming over La-promoted Ni/SBA-16 catalyst for syngas production: catalytic structure and process activity investigation. Int. J. Hydrog. Energy 48 (16), 6262–6274.
Kumar, R., Kumar, A., Pal, A., 2024. Simulation modelling of hydrogen production from steam reforming of methane and biogas. Fuel 362, 130742.
Kwon, Y., Eichler, J.E., Mullins, C.B., 2022. $NiAl_2O_4$ as a beneficial precursor for Ni/Al_2O_3 catalysts for the dry reforming of methane. J. CO2 Util. 63, 102112.
Lanre, M.S., Abasaeed, A.E., Fakeeha, A.H., Ibrahim, A.A., Al-Awadi, A.S., Jumah, A.B., Al-Mubaddel, F.S., Al-Fatesh, A.S., 2022. Lanthanum–cerium-modified nickel catalysts for dry reforming of methane. Catalysts 12 (7), 715.
Leba, A., Yıldırım, R., 2020. Determining most effective structural form of nickel-cobalt catalysts for dry reforming of methane. Int. J. Hydrog. Energy 45 (7), 4268–4283.
Liu, W., Li, L., Zhang, X., Wang, Z., Wang, X., Peng, H., 2018. Design of Ni-ZrO_2@ SiO_2 catalyst with ultra-high sintering and coking resistance for dry reforming of methane to prepare syngas. J. CO_2 Util. 27, 297–307.
Mabaleha, S.S., Gholizadeh, F., Kalita, P., 2023. Recent advances in Ni-based stable catalysts for methane dry reforming: stable catalysts' preparation review. Mol. Catal. 547, 113398.
Manan, W.N., Wan Isahak, W.N.R., Yaakob, Z., 2022. CeO_2-based heterogeneous catalysts in dry reforming methane and steam reforming methane: a short review. Catalysts 12 (5), 452.
Mesrar, F., Kacimi, M., Liotta, L.F., Puleo, F., Ziyad, M., 2018. Syngas production from dry reforming of methane over ni/perlite catalysts: effect of zirconia and ceria impregnation. Int. J. Hydrog. Energy 43 (36), 17142–17155.
Moghaddam, S.V., Rezaei, M., Meshkani, F., Daroughegi, R., 2018. Carbon dioxide methanation over Ni-M/Al_2O_3 (M: Fe, CO, Zr, La and Cu) catalysts synthesized using the one-pot sol-gel synthesis method. Int. J. Hydrog. Energy 43 (34), 16522–16533.
Mokheimer, E.M.A., Shakeel, M.R., Harale, A., Paglieri, S., Mansour, R.B., 2024. Fuel reforming processes for hydrogen production. Fuel 359, 130427.
Mourhly, A., Kacimi, M., Halim, M., Arsalane, S., 2020. New low cost mesoporous silica (MSN) as a promising support of Ni-catalysts for high-hydrogen generation via dry reforming of methane (DRM). Int. J. Hydrog. Energy 45 (20), 11449–11459.
Oni, B.A., Tomomewo, O.S., Sanni, S.E., Ojo, V.O., 2023. "Dry reforming of methane with CO_2 over Co-La1− xCaxNiO_3 perovskite-type oxides supported on ZrO_2". Materials Today. Communications 36, 106802.
Pan, C., Guo, Z., Dai, H., Ren, R., Chu, W., 2020. Anti-sintering mesoporous Ni–Pd bimetallic catalysts for hydrogen production via dry reforming of methane. Int. J. Hydrog. Energy 45 (32), 16133–16143.
Pompeo, F., Gazzoli, D., Nichio, N.N., 2009. Stability improvements of Ni/α-Al_2O_3 catalysts to obtain hydrogen from methane reforming. Int. J. Hydrog. Energy 34 (5), 2260–2268.
Poursadegh, F., 2023. Revolutionizing catalyst development–a comprehensive review of the past, present, and future of nanotechnologies in synthesis and development of new catalysts. Int. J. Mod. Dev. Eng. Sci. 2 (6), 5–11.
Ranjekar, A.M., Yadav, G.D., 2021. Dry reforming of methane for syngas production: a review and assessment of catalyst development and efficacy. J. Indian Chem. Soc. 98 (1), 100002.
Reshetenko, T.V., Avdeeva, L.B., Khassin, A.A., Kustova, G.N., Ushakov, V.A., Moroz, E. M., Shmakov, A.N., Kriventsov, V.V., Kochubey, D.I., Pavlyukhin, Y.T., Chuvilin, A. L., Ismagilov, Z.R., 2004. Coprecipitated iron-containing catalysts (Fe-Al_2O_3, Fe-Co-Al_2O_3, Fe-Ni-Al_2O_3) for methane decomposition at moderate temperatures: I. Genesis of calcined and reduced catalysts. Appl. Catal. A: Gen. 268 (1), 127–138.
Sadeq Al-Fatesh, A., Olajide Kasim, S., Aidid Ibrahim, A., Hamza Fakeeha, A., Elhag Abasaeed, A., Alrasheed, R., Ashamari, R., Bagabas, A., 2019. Combined magnesia, ceria and nickel catalyst supported over γ-alumina doped with titania for dry reforming of methane. Catalysts 9 (2), 188.
Salehi, S., Alavi, S.M., Rezaei, M., Akbari, E., Varbar, M., 2024. Syngas production from dry reforming of glycerol by the NiO/M-Al_2O_3 catalysts: Effect of various support promoters and various ZrO2 content. J. CO2 Util. 81, 102737.
Selvarajah, K., Phuc, N.H.H., Abdullah, B., Alenazey, F., Vo, D.-V.N., 2016. Syngas production from methane dry reforming over Ni/Al_2O_3 catalyst. Res. Chem. Intermed. 42 (1), 269–288.
Setiabudi, H., Lim, K., Ainirazali, N., Chin, S., Kamarudin, N., 2017. CO_2 reforming of CH_4 over Ni/SBA-15: influence of Ni loading on the metal-support interaction and catalytic activity. J. Mater. Environ. Sci. 8 (2), 573–581.
Singha, R.K., Shukla, A., Yadav, A., Adak, S., Iqbal, Z., Siddiqui, N., Bal, R., 2016. Energy efficient methane tri-reforming for synthesis gas production over highly coke resistant nanocrystalline Ni–ZrO_2 catalyst. Appl. Energy 178, 110–125.
Sokolov, S., Radnik, J., Schneider, M., Rodemerck, U., 2017. Low-temperature CO_2 reforming of methane over Ni supported on ZnAl mixed metal oxides. Int. J. Hydrog. Energy 42 (15), 9831–9839.
Sun, D., Du, Y., Wang, Z., Zhang, J., Li, Y., Li, J., Kou, L., Li, C., Li, J., Feng, H., 2020. Effects of CaO addition on Ni/CeO_2–ZrO_2–Al_2O_3 coated monolith catalysts for steam reforming of N-decane. Int. J. Hydrog. Energy 45 (33), 16421–16431.
Taherian, Z., Khataee, A., Han, N., Orooji, Y., 2022. Hydrogen production through methane reforming processes using promoted-Ni/mesoporous silica: a review. J. Ind. Eng. Chem. 107, 20–30.
Therdthianwong, S., Therdthianwong, A., Siangchin, C., Yongprapat, S., 2008. Synthesis gas production from dry reforming of methane over Ni/Al_2O_3 stabilized by ZrO_2. Int. J. Hydrog. Energy 33 (3), 991–999.
Torrez-Herrera, J.J., Korili, S.A., Gil, A., 2021. Recent progress in the application of Ni-based catalysts for the dry reforming of methane. Catal. Rev. 1–58.
ul Hasnain, S.M.W., Farooqi, A.S., Ayodele, B.V., Farooqi, A.S., Sanaullah, K., Abdullah, B., 2024. Advancements in Ni and Co-based catalysts for sustainable syngas production via Bi-reforming of methane: a review of recent advances. J. Clean. Prod. 434, 139904.
Usman, M., Daud, W.W., Abbas, H.F., 2015. Dry reforming of methane: Influence of process parameters—a review. Renew. Sustain. Energy Rev. 45, 710–744.
Velisoju, V.K., Virpurwala, Q.J.S., Attada, Y., Bai, X., Davaasuren, B., Hassine, M.B., Yao, X., Lezcano, G., Kulkarni, S.R., Castano, P., 2023. Overcoming the kinetic and deactivation limitations of Ni catalyst by alloying it with Zn for the dry reforming of methane. J. CO_2 Util. 75, 102573.
Vogt, C., Kranenborg, J., Monai, M., Weckhuysen, B.M., 2019. Structure sensitivity in steam and dry methane reforming over nickel: activity and carbon formation. ACS Catal. 10 (2), 1428–1438.
Walker, D.M., Pettit, S.L., Wolan, J.T., Kuhn, J.N., 2012. Synthesis gas production to desired hydrogen to carbon monoxide ratios by tri-reforming of methane using Ni–MgO–(Ce,Zr)O_2 catalysts. Appl. Catal. A: Gen. 445-446, 61–68.
Wang, Y., Li, L., Cui, C., Costa, P.D., Hu, C., 2022. The effect of adsorbed oxygen species on carbon-resistance of Ni-Zr catalyst modified by Al and Mn for dry reforming of methane. Catal. Today 384, 257–264.
Wang, L., Wang, F., 2022. Design strategy, synthesis, and mechanism of Ni catalysts for methane dry reforming reaction: recent advances and future perspectives. Energy Fuels 36 (11), 5594–5621.
Wang, Y., Zhang, R., Yan, B., 2022. Ni/Ce0. 9Eu0. 1O1. 95 with enhanced coke resistance for dry reforming of methane. J. Catal. 407, 77–89.
Yahi, N., Menad, S., Rodríguez-Ramos, I., 2015. Dry reforming of methane over Ni/CeO_2 catalysts prepared by three different methods. Green. Process. Synth. 4 (6), 479–486.
Yan, X., Du, X.-H., Jing, L., Peng, W., Jie, Z., Ge, F.-J., Jun, Z., Ming, S., Zhu, W.-Y., 2019. A comparison of Al_2O_3 and SiO_2 supported Ni-based catalysts in their performance for the dry reforming of methane. J. Fuel Chem. Technol. 47 (2), 199–208.

Yentekakis, I.V., Panagiotopoulou, P., Artemakis, G., 2021. A review of recent efforts to promote dry reforming of methane (DRM) to syngas production via bimetallic catalyst formulations. Appl. Catal. B Environ. 296, 120210.
Yusuf, M., Farooqi, A., Keong, L., Hellgardt, K., Abdullah, B., 2020. Latest trends in Syngas production employing compound catalysts for methane dry reforming. IOP Conference Series: Materials Science and Engineering. IOP Publishing.
Zhang, X., Deng, J., Lan, T., Shen, Y., Qu, W., Zhong, Q., Zhang, D., 2022. Coking-and sintering-resistant Ni nanocatalysts confined by active BN edges for methane dry reforming. ACS Appl. Mater. Interfaces 14 (22), 25439–25447.
Zhang, T., Liu, Z., Zhu, Y.-A., Liu, Z., Sui, Z., Zhu, K., Zhou, X., 2020. Dry reforming of methane on Ni-Fe-MgO catalysts: influence of Fe on carbon-resistant property and kinetics. Appl. Catal. B: Environ. 264, 118497.
Zhang, X., Vajglova, Z., Mäki-Arvela, P., Peurla, M., Palonen, H., Murzin, D.Y., Tungatarova, S.A., Baizhumanova, T.S., Aubakirov, Y.A., 2021. Mono-and bimetallic Ni− Co catalysts in dry reforming of methane. ChemistrySelect 6 (14), 3424–3434.
Zhang, Z., Zhang, Y., Liu, L., 2024. Role and mechanism of calcium-based catalysts for methane dry reforming: a review. Fuel 355, 129329.
Zhang, M., Zhang, J., Wu, Y., Pan, J., Zhang, Q., Tan, Y., Han, Y., 2019. Insight into the effects of the oxygen species over Ni/ZrO_2 catalyst surface on methane reforming with carbon dioxide. Appl. Catal. B: Environ. 244, 427–437.
Zhou, R., Mahinpey, N., 2023. A review on catalyst development for conventional thermal dry reforming of methane at low temperature. Can. J. Chem. Eng.
Zolghadri, S., Kiani, M.R., Rahimpour, M.R., 2024. Enhanced hydrogen production in steam methane reforming: comparative analysis of industrial catalysts and process optimization. J. Energy Inst., 101541
Zuo, Z., Liu, S., Wang, Z., Liu, C., Huang, W., Huang, J., Liu, P., 2018. Dry reforming of methane on single-site Ni/MgO catalysts: importance of site confinement. ACS Catal. 8 (10), 9821–9835.